High performance electro-optic modulator based on thin-film lithium niobate*

LIU Leshu, LIU Ning, ZHANG Jianfa, ZHU Zhihong, and LIU Ken**

College of Advanced Interdisciplinary Studies & Hunan Provincial Key Laboratory of Novel Nano-Optoelectronic Information Materials and Devices, National University of Defense Technology, Changsha 410073, China

(Received 30 March 2022; Revised 4 May 2022)

Electro-optic (EO) modulator plays a very critical role in the optical communication systems. Here, we report a stimulated thin-film lithium niobate (LN) modulator with a half-wave voltage-length product of 1.8 V·cm, which can successfully achieve modulation and demodulation of a 1 GHz sinusoidal signal with an amplitude of 5 V in experiment. The optical loss caused by metal electrodes is reduced by optimizing the waveguide structure and depositing silica onto the waveguide, and group-velocity matching and characteristic impedance matching are achieved by optimizing the buffer silica layer and the electrode structure for larger bandwidth, which simultaneously improves the modulation efficiency and bandwidth performance. Our work demonstrated here paves a foundation for integrated photonics.

Document code: A **Article ID:** 1673-1905(2022)10-0583-5

DOI https://doi.org/10.1007/s11801-022-2049-y

Electro-optic (EO) modulators, converting electrical signals into optical signals, are extremely critical devices in the optical interconnection networks for long-distance and high-speed information transmission[1,2]. In order to meet people's needs for high-speed optical interconnection, especially the needs for new business scenarios such as the artificial intelligence, the internet of things and 5G, modulators based on many photonic platforms have been explored, such as lithium niobate (LN)[3-6], silicon[7,8], III-V semiconductors[9,10], polymers[11,12], indium phosphide[13,14], graphene[15,16], plasmon[17,18]. Among them, LN is the most widely used material for commercial EO modulators, which is due to its excellent EO properties of linear EO response (Pockels effect), large EO coefficient (30.8 pm/V), wide optically transparent window (0.4—5 μm) and stable physical and chemical properties[19]. However, traditional LN waveguides in EO modulators are usually fabricated by titanium (Ti) diffusion or proton exchange methods[20,21], which have weak confinement for the optical field (Δn < 0.02). Large optical mode size means that the metal electrodes must be placed far away from the optical waveguides to avoid excessive optical loss, usually resulting in a much larger footprint and lower modulation efficiency.

The emergence of thin-film lithium niobate (TFLN) effectively solves the dilemma of bulk LN and the excellent EO properties of bulk LN are preserved.

The commercial LN-on-insulator (LNOI) wafer is fabricated by smart cutting method[22] through which LN film is bonded directly onto a low-refractive-index substrate. Compared with the traditional Ti diffusion waveguides, LN waveguides fabricated by dry etching have a large refractive index difference (Δn>0.7) between the cladding and the core, resulting in a smaller mode area and tighter optical confinement. Many EO modulators based on TFLN have been demonstrated[23-25]. However, the non-ideal waveguide morphology after dry etching, low overlap between the electric and optical fields, group-velocity mismatch and impedance mismatch limit the bandwidth, footprint, and modulation efficiency, which is an urgent issue to be solved for modulator improvement.

In this paper, we demonstrate a TFLN Mach-Zehnder modulator (MZM) (Fig.1(a)) that meets the requirements of large modulation bandwidth, small footprint and high modulation efficiency simultaneously, which is fabricated by Ar^+-based inductively coupled plasma (ICP) etching. It can achieve modulation and demodulation of a 1 GHz sinusoidal signal with an amplitude of 5 V and the stimulated half-wave-voltage length product (or modulation efficiency) is 1.8 V·cm. We make the following two improvements to address the shortcomings of traditional modulators based on TFLN. Firstly, optical loss of the LN waveguides is reduced by depositing a layer of silicon dioxide (SiO_2) after the waveguides and electrodes are prepared. Secondly, group-velocity matching between the optical field and the radio frequency (RF) field and characteristic impedance matching are realized to improve the bandwidth of the modulator by optimizing the electrode structure parameters and the thickness of the buffer SiO_2 layer.

* This work has been supported by the Science and Technology Planning Project of Hunan Province (Nos.2018JJ1033 and 2017RS3039).
** E-mail: liukener@163.com

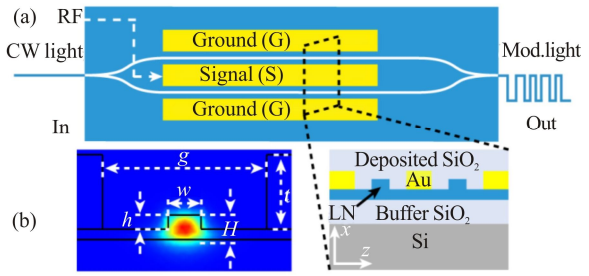

Fig.1 (a) Schematic diagram of the TFLN-MZM (The insert is the cross-sectional view of the modulator); (b) Field distribution of the TE_0 mode when the waveguide height is 380 nm and the waveguide width is 1 μm

The schematic of the device structure is shown in Fig.1(a). Fig.1(b) is the optical field distribution of the high-performance TFLN-MZM, where the thickness of x-cut LN (H) is 660 nm, the width (w) and the height (h) of ridge waveguide are 1 μm and 380 nm, respectively, the thickness of the electrode is 0.5 μm and the electrode gap (g) is 5 μm. Submicron-scale optical confinement is realized using those parameters, under which the electrodes are allowed to place closer to the waveguide and thereby improving the modulation efficiency.

In order to fabricate a high-performance TFLN EO modulator, we need to design a low-loss single-mode LN waveguide. First, the ridge waveguide height (h) is fixed to be 380 nm. Fig.2 shows the relationship between the effective refractive index and the waveguide width (w) for different transverse-electric (TE) optical modes. It can be seen from Fig.2 that the effective refractive index increases with the increase of the waveguide width. Furthermore, the three TE modes distribute mainly in the ridge waveguide when the waveguide width is more than 1 μm. However, the effective refractive indexes of the TE_1 and TE_2 modes are almost constant when the waveguide width is less than 1 μm, which means that the two TE modes mainly exist in the slab LN layer. When the two modes propagate in the slab layer, the optical energy will be almost completely absorbed by the metal electrodes. Only the fundamental TE_0 mode can be left propagating in the ridge waveguide when the waveguide width is set to less than 1 μm. So, the optimal waveguide width is set to be 1 μm when the modulator operates in the single-mode state.

Second, when the waveguide width is set to be 1 μm, the relationship between the mode area of the fundamental TE mode and the waveguide height is shown in Fig.3. As the waveguide height increases, the mode area becomes smaller, which means the optical confinement effect of the waveguide is enhanced. The mode area does not change much when the waveguide height is more than 380 nm, indicating that the 380-nm-high waveguide is enough for tight optical confinement. After comprehensive analysis, the width and height of the ridge waveguide in our later simulation are fixed to be 1 μm and 380 nm, respectively. Under this situation, the effective refractive index of the TE_0 mode is calculated to be 1.88.

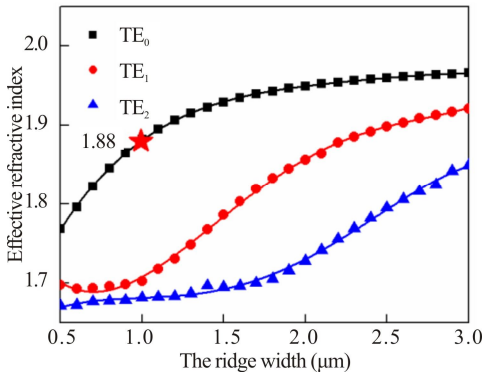

Fig.2 Relationship between the effective refractive index of three TE modes and the ridge width (The ridge height is set to be 380 nm)

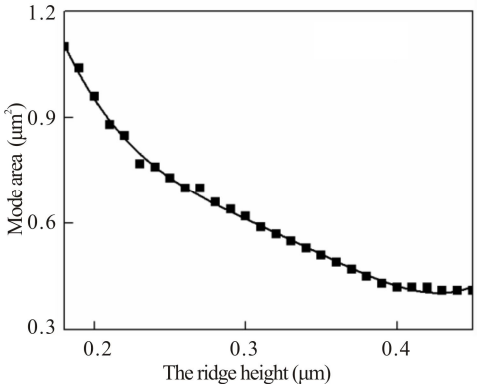

Fig.3 Relationship between the mode area and the ridge height (The ridge width is set to be 1 μm)

There is always a trade-off between the half-wave-voltage length product and the modulation bandwidth. When the electrodes are placed closer to the LN waveguide, a smaller half-wave-voltage length product can be realized, thus improving the modulation performance. However, closer electrode gap also means more optical loss caused by the absorption of the metal electrodes. To avoid excessive optical loss, the electrode gap is usually larger than 10 μm[24]. Therefore, we demonstrate that a layer of 1-μm-thick SiO_2 be deposited after the LN waveguides and the Au electrodes are fabricated for reducing the optical loss caused by the electrodes. It can be seen from the simulation results in Fig.4 that the optical loss caused by the electrodes is reduced after depositing a layer of SiO_2 when the electrode gap varies from 2.0 μm to 4.0 μm.

Another difficulty that limits the performance of the modulator is the group-velocity mismatching and characteristic impedance mismatching between the optical field and the electric field. Because the dielectric constants of LN at optical frequencies and RF are 5 and 28[1],

respectively, they cannot propagate at same speed and result in phase mismatch. The characteristic impedance matching ensures the RF can pass through the interface between the modulator and the external loads. The standard impedance of external loads is typically 50 Ω, which means the characteristic impedance of electrodes should be as close to 50 Ω as possible. For TFLN-MZM, a large part of the electric field distributes in the substrate, so we can achieve group-velocity matching and characteristic impedance matching by optimizing the thickness of the buffer SiO_2 layer and the parameters of the co-plane electrodes. The relationships between the effective refractive index/characteristic impedance and the ground electrode width are shown in Fig.5(a). We can find the change of the ground electrode width has a minimal effect on the effective refractive index and characteristic impedance. When the ground electrode width is set to be 36 μm, the effective refractive index and characteristic impedance are 1.86 and 51 Ω, respectively. When setting the ground electrode width to 36 μm, the relationships between the effective refractive index/characteristic impedance and the signal electrode width are shown in Fig.5(b). When the width of the signal electrode is 14 μm, the effective refractive index and characteristic impedance are close to 1.88 and 50 Ω, respectively. After analyzing Fig.4(a) and Fig.4(b), we set the width of signal electrode and ground electrode to be 14 μm and 36 μm, respectively.

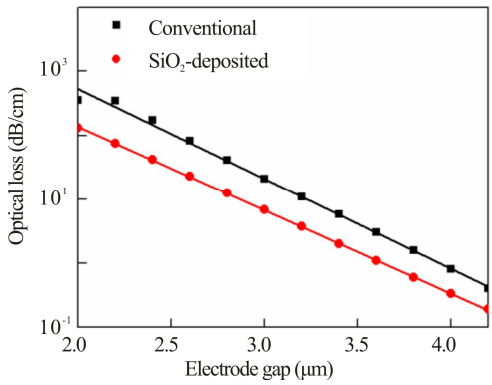

Fig.4 Relationship between the optical loss and the electrode gap for the conventional TFLN-MZM and the SiO_2-deposited TFLN-MZM

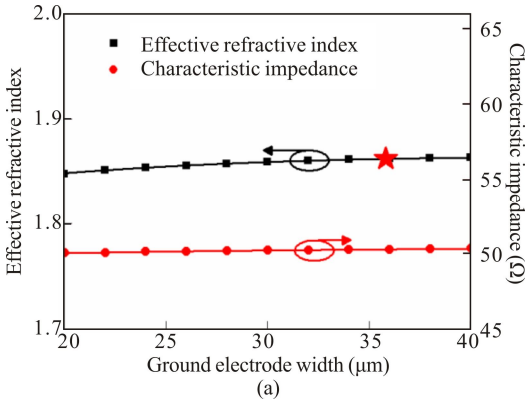

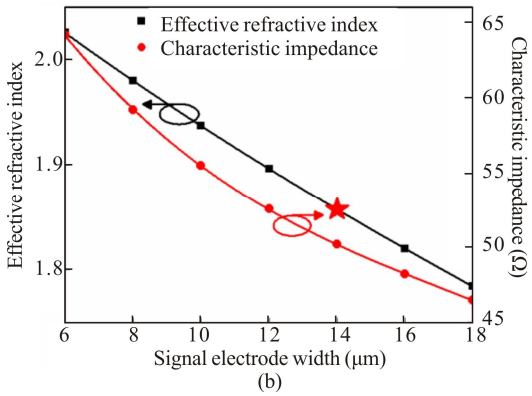

Fig.5 Relationship between the effective refractive index/characteristic impedance and (a) the ground electrode width and (b) the signal electrode width

Then, we optimized the thicknesses of the buffer layer and the electrode to realize the group-velocity matching and characteristic impedance matching, which are close to 1.88 and 50 Ω. As shown in Fig.6(a) and Fig.6(b), when the thicknesses of the buffer layer and electrode are 0.8 μm and 0.5 μm, respectively, the group-velocity and characteristic impedance matching can be realized.

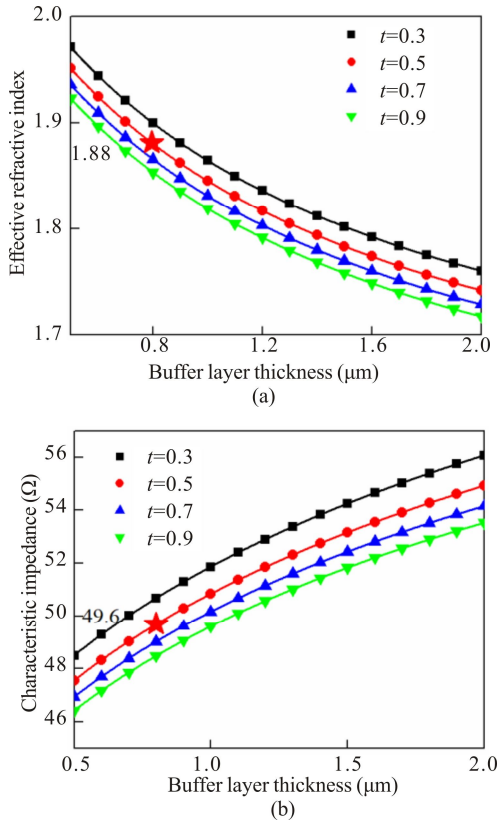

Fig.6 (a) Relationship between the effective refractive index and the buffer SiO_2 layer thickness; (b) Relationship between the characteristic impedance and the buffer SiO_2 layer thickness

Finally, we simulated the transmittance versus modulator voltage of the device. According to the electro-optical

effect formula of LN, we obtained the relationship between the transmittance and voltage, as shown in Fig.7. We can see that the transmittance is close to 0 and 1 when the voltage is −3.4 V and 0.2 V, respectively and the half-wave voltage V_π is 3.6 V. In the real experiment, the existing signal source in our laboratory can only take some discrete voltage and cannot be arbitrarily selected. So we chose 5 V, which is the closest to 3.4 V.

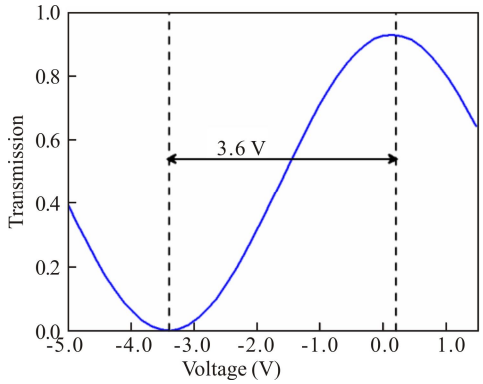

Fig.7 Transmittance as a function of voltage

Fig.8 shows the device fabrication process. A commercial x-cut LNOI wafer from NANOLN is shown in Fig.8(a), where a 660-nm-thick TFLN layer is bonded on the top of the SiO_2/Si-stack substrate. Fig.8(b) shows the fabrication process of etching mask. A layer of photoresist is spun coat on the top of the LNOI wafer. Then, the waveguide pattern is defined on the photoresist by lithography and transferred into the LN layer by using Ar^+-based ICP etching (Fig.8(c)). The residual resist is removed by using acetone, isopropanol, and deionized water sequentially (Fig.8(d)). Fig.8(e) and Fig.8(f) show the fabrication process of the electrodes. The electrode patterns are first defined in the same way as in step (b). The electrodes (6-nm Cr and 0.5-μm Au) are fabricated along the LN waveguide by using electron beam evaporation (Fig.8(e)) and lift-off (Fig.8(f)). A layer of 1-μm-thick SiO_2 is deposited on the waveguides and electrodes by using plasma enhanced chemical vapor deposition (PECVD) (Fig.8(g)). Finally, sticking the fabricated modulator on the top of a printed circuit board (PCB), connect the modulator's electrodes with the PCB's contact pad by using wire bonding process (Fig.8(h)).

The fabricated modulator is shown in Fig.9(a). Because the efficiency of fiber coupling with on-chip system will affect our device testing, we tested the performance of our device based on our research group's previous work on efficient coupling of fiber and integrated photonic device[26]. The sinusoidal signal with an amplitude of 5 V generated by a high-speed signal source is loaded on the modulator. The modulated optical wave passes through a high-speed photodetector and is displayed on the oscilloscope. The waveform on the oscilloscope shows the SiO_2-deposited TFLN-MZM can respond well to the loaded 1 GHz microwave signal with an amplitude of 5 V, as shown in Fig.9(b). However, the device has relatively high insertion loss of about 10 dB, which is mainly due to the rough side wall of the etched LN waveguide and limits the bandwidth. This is one of the problems that we are going to solve next.

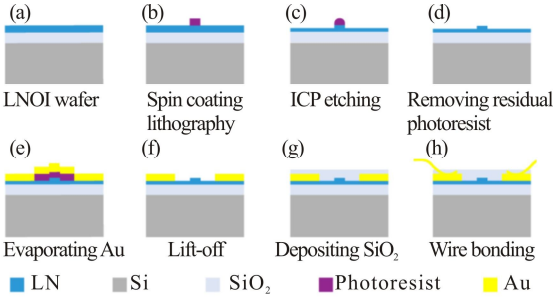

Fig.8 Device fabrication process: (a) The x-cut LNOI wafer; (b) The waveguide pattern defined in photoresist by lithography; (c) Transferring the waveguide pattern into the LN film by ICP etching; (d) Removing the residual resist; (e) Evaporating 0.5-μm-thick metal electrodes along the LN waveguide; (f) Lift-off; (g) Depositing 1-μm-thick SiO_2 on the top of electrode and waveguides; (h) Wire bonding (Au line)

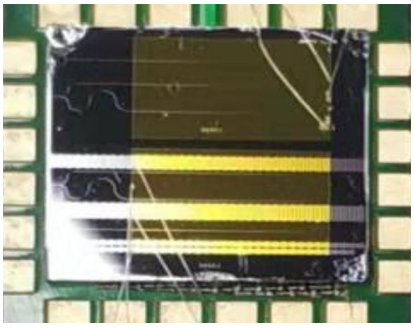

(a)

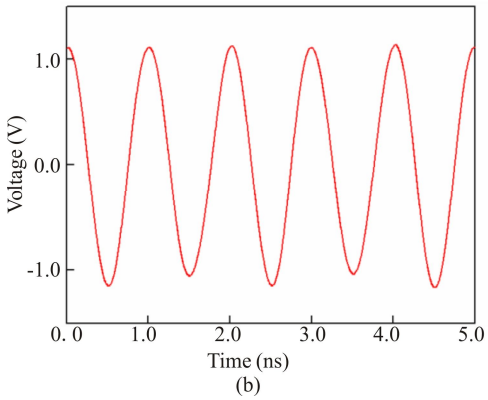

(b)

Fig.9 (a) The photography of the fabricated TFLN-MZM; (b) The measured result when a sinusoidal signal with an amplitude of 5 V is loaded

In summary, we propose a modulator that satisfies high modulation efficiency, high speed, and small size simultaneously. The optical loss can be reduced by

depositing 1-μm-thick SiO_2 onto the waveguides and electrodes, which further improves the modulation efficiency. There is always a large difference in group velocity between the optical frequency and RF. In our designed TFLN-MZM, the group velocity and characteristic impedance matching are realized by optimizing the substrate thickness and electrode structure parameters without sacrificing the EO modulation efficiency. Combining the above two points, high performance EO modulator based on TFLN is realized, which has a stimulated half-wave voltage-length product of 1.8 V·cm and can successfully achieve modulation and demodulation of a 1 GHz sinusoidal signal with an amplitude of 5 V in experiment.

Statements and Declarations

The authors declare that there are no conflicts of interest related to this article.

References

[1] WANG C, ZHANG M, CHEN X, et al. Integrated lithium niobate electro-optic modulators operating at CMOS-compatible voltages[J]. Nature, 2018, 562(7725)：101-104.

[2] WANG C, ZHANG M, STREN B, et al. Nanophotonic lithium niobate electro-optic modulators[J]. Optics express, 2018, 26(2)：1547-1555.

[3] XU M, HE M, ZHU Y, et al. Integrated thin film lithium niobate Fabry-Perot modulator[Invited][J]. Chinese optics letters, 2021, 19(6)：060003.

[4] HE M, XU M, REN Y, et al. High-performance hybrid silicon and lithium niobate Mach-Zehnder modulators for 100 Gbit s^{-1} and beyond[J]. Nature photonics, 2019, 13(5)：359-364.

[5] DESIATOV B, SHAMS-ANSARI A, ZHANG M, et al. Ultra-low-loss integrated visible photonics using thin-film lithium niobate[J]. Optica, 2019, 6(3)：380-384.

[6] KHAREL P, REIMER C, LUKE K, et al. Breaking voltage-bandwidth limits in integrated lithium niobate modulators using micro-structured electrodes[J]. Optica, 2021, 8(3)：357-363.

[7] XU H, LI X, XIAO X, et al. High-speed silicon modulator with band equalization[J]. Optics letters, 2014, 39(16)：4839-4842.

[8] CHMIELAK B, WALDOW M, MATHEISEN C, et al. Pockels effect based fully integrated, strained silicon electro-optic modulator[J]. Optics express, 2011, 19(18)：17212-17219.

[9] BHASKER P, NORMAN J, BOWERS J, et al. Intensity and phase modulators at 1.55 μm in GaAs/AlGaAs layers directly grown on silicon[J]. Journal of lightwave technology, 2018, 36(158)：4205-4210.

[10] WANG S, WANG L, ZHAO L, et al. Compact InGaAsP/InP asymmetric Mach-Zehnder coupled square ring modulator[J]. IEEE photonics technology letters, 2017, 29(16)：1312-1315.

[11] MIURA H, QIU F, SPRING A M, et al. High thermal stability 40 GHz electro-optic polymer modulators[J]. Optics express, 2017, 25(23)：28643-28649.

[12] QIU F, HAN Y. Electro-optic polymer ring resonator modulators[Invited][J]. Chinese optics letters, 2021, 19(4)：041301.

[13] QIAN G, NIU B, ZHAO W, et al. CL-TWE Mach-Zehnder electro-optic modulator based on InP-MQW optical waveguides[J]. Chinese optics letters, 2019, 17(6)：061301.

[14] OGISO Y, OZAKI J, UEDA Y, et al. Over 67 GHz bandwidth and 1.5 V V_π InP-based optical IQ modulator with n-i-p-n heterostructure[J]. Journal of lightwave technology, 2017, 35(8)：1450-1455.

[15] LIU M, YIN X, ULIN-AVILA E, et al. A graphene-based broadband optical modulator[J]. Nature, 2011, 474(7349)：64-67.

[16] PHARE C T, LEE Y D, CARDENAS J, et al. Graphene electro-optic modulator with 30 GHz bandwidth[J]. Nature photonics, 2015, 9(8)：511-514.

[17] LIANG Z X, XU C P, ZHU A J, et al. Hybrid photonic-plasmonic electro-optic modulator for optical ring network-on-chip[J]. Optik, 2020, 210：164503.

[18] TIBALDI A, GHOMASHI M, BERTAZZI F, et al. Plasmonic-organic hybrid electro/optic Mach-Zehnder modulators：from waveguide to multiphysics modal-FDTD modeling[J]. Optics express, 2020, 28(20)：29253-29271.

[19] QI Y, LI Y. Integrated lithium niobate photonics[J]. Nanophotonics, 2020, 9(6)：1287-1320.

[20] THIELE F, BRUCH F V, QUIRING V, et al. Cryogenic electro-optic polarisation conversion in titanium in-diffused lithium niobate waveguides[J]. Optics express, 2020, 28(20)：28961-28968.

[21] PALIWAL A, SHARMA A, GUO R, et al. Electro-optic (EO) effect in proton-exchanged lithium niobate：towards EO modulator[J]. Applied physics B, 2019, 125(7)：115.

[22] ZHU D, SHAO L, YU M, et al. Integrated photonics on thin-film lithium niobate[J]. Advanced optics photonics, 2021, 13(2)：242-352.

[23] REN T, ZHANG M, WANG C, et al. An integrated low-voltage broadband lithium niobate phase modulator[J]. IEEE photonics technology letters, 2019, 31(11)：889-892.

[24] BAHADORI M, GODDARD L L, GONG S. Fundamental electro-optic limitations of thin-film lithium niobate microring modulators[J]. Optics express, 2020, 28(9)：13731-13749.

[25] HONARDOOST A, JUNEGHANI F A, SAFIAN R, et al. Towards subterahertz bandwidth ultracompact lithium niobate electrooptic modulators[J]. Optics express, 2019, 27(5)：6495-6501.

[26] LIU N, ZHANG J, ZHU Z, et al. Efficient coupling between an integrated photonic waveguide and an optical fiber[J]. Optics express, 2021, 29(17)：27396-27403.